Conclusions: This study shows that MSI is feasible on FNA cell block material and can be helpful in obtaining quantitative data from multiple antibodies used on a single slide, which may be advantageous in FNA samples with limited material and may potentially be helpful in the cytologic distinction of RLH and FL.

1958 Automated Brightfield Dual Color In Situ Hybridization for Detection of *MDM2* Gene Amplification in Sarcomas

W Zhang, A McElhinny, A Nielsen, M Wang, M Miller, S Singh, R Rueger, B Rubin, RR Tubbs, P Roche, P Wu, L Pestic-Dragovich. Ventana Medical Systems, Inc., Tucson, AR; Roche Diagnostics GmbH, Penzberg, Germany; Cleveland Clinic, Cleveland, OH.

Background: The human homologue of the mouse double minute 2 (*MDM2*) oncogene is amplified in about 20% of sarcomas. Measurement of *MDM2* amplification can aid in classification, and may provide predictive value for recently formulated therapies targeting *MDM2*. Here, we have developed and validated an automated brightfield dual color *in situ* hybridization application for *MDM2* gene amplification in sarcomas.

Design: A repeat-depleted *MDM2* probe was constructed to target the *MDM2* gene region at 12q15. A chromosome 12-specific probe (Chr 12) was generated from pα12H8 plasmid. The ISH assay was developed with dinitrophenyl-labeled *MDM2* probe and digoxigenin-labeled Chr 12 probe on Ventana Medical Systems, Inc. automated slide staining platforms. The specificity of the *MDM2* and Chr 12 probes was demonstrated on metaphase spreads, and further validated against controls including normal human tonsil and known *MDM2*-amplified samples. The assay performance was evaluated on a cohort of 68 FFPE specimens using a conventional brightfield microscope.

Results: Simultaneous hybridization and signal detection for *MDM2* and Chr 12 demonstrated both DNA targets in the same cells. 66 of 68 cases had interpretable signals for *MDM2* and Chr 12. While all four lipomas were nonamplified and eusomic, *MDM2* amplification was noted in 81% (21/26) of well-differentiated liposarcomas. *MDM2* amplification was observed in 1 of 8 osteosarcomas; 3 demonstrated Chr 12 aneusomy; and the other 4 were non-amplified. *MDM2* amplification was present in 1 of 4 chondrosarcomas; the remaining 3 cases had normal *MDM2* and Chr 12 copy numbers. 11 of 13 synovial sarcomas displayed no evidence of *MDM2* amplification on most cells; the other two had Chr 12 aneusomy. In pleomorphic sarcoma, not otherwise specified (malignant fibrous histiocytoma), *MDM2* was amplified in 31% (4/12) interpretable cases, while 92% (11/12) were aneusomy for Chr 12 . One alveolar rhabdomyosarcoma and two embryonal rhabdomyosarcoma cases had low level aneusomy of Chr 12.

Conclusions: The use of ISH *MDM2*/Chr 12 assay allows the simultaneous analyses of the two DNA targets within the context of tissue morphology. This method combines the advantage of brightfield microscopy with fully automated analysis and has the potential for routine application in surgical pathology.

Ultrastructural

1959 Electron Microscopic Finding in Skin Biopsies from Patients with Danon Disease

J Alroy, R Pfannl, D Slavov, MRG Taylor. Tufts University School of Medicine, Boston, MA; Tufts Cumming's School of Veterinary Medicine, Grafton, MA; Tufts Medical Center, Boston, MA; University of Colorado, Aurora, CO.

Background: Danon Disease is an X-linked lysosomal storage disease. It is due to primary deficiency of lysosomal-associated membrane protein-2 (LAMP-2). LAMP-2 is an important regulator of maturation of both autophagosomes and phagosomes. Deficiency of LAMP-2 results in accumulation of autophagosomes in multiple tissues and a phenotype triad of hypertrophic cardiomyopathy, myopathy, and mental retardation. A milder phenotype occurs in females. Clinical manifestation typically develops in boys in the first two decades of life. Skin biopsy is a useful cost effective tool for the diagnosis of other lysosomal storage diseases, but its role in Danon disease has not been studied.

Design: In this study we obtained skin biopsies from the forearms of a 24-years- old man and a 43-years-old woman and her 9-year-old son from two unrelated families. The diagnosis of Danon diseases was confirmed by DNA analysis and absent LAMP-2 protein in skin fibroblasts from both males. The 2-mm^2 biopsies were fixed in Trump's fixative and postfixed in 1% osmium tetroxide in sodium cacodylate buffer, stained with 5% uranyl acetate, dehydrated and embedded in resin (Epon-812). Thick sections (1um) were stained with toluidine blue. Thin sections were cut at 50-70nm, stained with uranyl acetate and lead citrate, and photographed with a transmission electron microscope.

Results: Few large membrane bound electron lucent vacuoles, i.e., lysosomes were noted in myelinated axons and in some smooth muscle and fewer in perineural cells. Some fibroblasts contain both electron lucent lysosomes as well as lysosomes that contain electron dense material. Rare storage of lamellated membrane structures was noted in unmyelinated axons.

Conclusions: These unique morphological findings demonstrate the usefulness of skin biopsies in the diagnosis of Danon disease. They are distinct from those seen in patients with muscopolysaccharidosis, with glycolipids and oligosacchardide storage diseases, neuronal ceroid lipofuscinosis, as well as various myopathies.

1960 Birt-Hogg-Dubé Renal Tumors Express Characteristic Ultrastructural Features Which Distinguish Them from Other Hereditary and Sporadic Renal Neoplasms

S Hebert-Magee, MJ Merino, WM Linehan, M Tsokos. National Institutes of Health, Bethesda, MD.

Background: Birt-Hogg-Dubé (BHD) syndrome is an autosomal dominant genodermatosis characterized by a predisposition to hamartomatous cutaneous lesions, spontaneous pneumothoraces, pulmonary cysts and renal neoplasms. Light microscopic evaluation of the BHD renal tumors has suggested the existence of various morphologies including chromophobe, oncocytic and hybrid variants. To date, there has been no ultrastructural analysis of these tumors.

Design: We utilized the collection of BHD renal neoplasms at our institution and evaluated their ultrastructural features in comparison to those of sporadic or familial chromophobe carcinomas and oncocytomas. Eleven cases were evaluated, 5 of which BHD associated and 6 sporadic or familial.

Results: We found that all 5 BHD renal tumors expressed a hybrid chromophobe/oncocytic phenotype, which was apparent in individual tumor cells. Specifically, tumor cells exhibited numerous mitochondria (oncocytic phenotype) and microvesicles (chromophobe phenotype). The mitochondria were similar to those described in sporadic oncocytomas, i.e. small and round with lamellar cristae. Many tumors contained cells with apical villi and formation of lumina and with elaborate cytoplasmic interdigitations. Sporadic or familial tumors without BHD mutation were of pure morphology, either oncocytic (5 tumors), or chromophobe (1 tumor). The chromophobe tumor also had many mitochondria, but they were of variable size including large ones and had the characteristic tubulovesicular cristae. Luminal differentiation was present in the chromophobe carcinoma, but not in the oncocytomas. All but one oncocytomas had focal intracytoplasmic aggregates of filaments and consisted of groups of cells surrounded by thick basement membrane. The cytoplasmic contours were smooth, except in one tumor, which showed basal interdigitations. Lipid droplets and glycogen were present but not abundant in all tumors.

Conclusions: Our study showed that all BHD renal tumors exhibit a hybrid chromophobe/oncocytic ultrastructural phenotype, which distinguishes them from oncocytic or chromophobe tumors in sporadic or other familial settings. Therefore, electron microscopy can be instrumental in identifying BHD patients without overt clinical manifestations.

1961 Fulminant Hepatic Failure and Giant Cell Hepatitis Associated with Paramyxoviral-Like Inclusions: Contribution of Electron Microscopy

J Hicks, SH Zhu, J Barrish. Texas Children's Hospital & Baylor College of Medicine, Houston, TX.

Background: Etiologic agents responsible for acute fulminant liver failure (AFLF) and giant cell hepatitis (GCH) are not readily identified. Paramyxovirus (PV) has been associated with AFLF and GCH in children and adults (NEJM 1991;324:455; UltraPath 2001;25:65). PV hepatitis is associated with giant cell transformation, cholestasis, bridging fibrosis, chronic hepatitis, and rapidly progressive fulminant liver disease. Time-consuming viral cultures may detect PV in some, but not all cases. PV PCR is not currently available. PV inclusions may be identified based upon ultrastructural features.

Design: 7 children with GCH and/or AFLF were studied (5M:2F, age range 6wks-11yrs, mean 7yrs). Liver biopsies and/or explants were available for evaluation. Tissue was submitted for viral cultures and viral PCR studies, and also available for routine and electron microscopic study. Histopathologic examination included H&E, PAS, PAS with diastase, trichrome, iron and copper staining. Immunocytochemistry for Adenovirus, CMV, HSV, EBV, Parvovirus and Hepatitis B were performed with most cases. Electron microscopy was performed.

Results: Liver biopsies and explants demonstrated giant cell transformation, ballooning degeneration, binucleate hepatocytes, cytoplasmic and canalicular cholestasis, pseudoacinar formation, and reactive and pyknotic nuclei. Occasional hepatocytes had eosinophilic glassine cytoplasm. There were frequent apoptotic hepatocytes and geographic necrosis. Chronic inflammatory infiltrates with only infrequent acute inflammatory cells were present. Immunocytochemistry failed to identify Adenovirus, CMV, HSV, EBV, Parvovirus and Hepatitis B. Electron microscopy identified viral inclusions within the cytoplasm of occasional hepatocytes. The viral inclusions were comprised of relatively large round to ovoid aggregates of fine filamentous, beaded substructures (14-20 nm width). Viral inclusions were interspersed with typical cell organelles. There were no intranuclear inclusions. The ultrastructural features are those associated with paramyxovirus. 4 cases subsequently had paramyxovirus identified by viral cultures.

Conclusions: Paramyxovirus is associated with an aggressive clinical course and rapidly progressive AFLF. Ultrastructural examination of liver biopsies/explants with GCH and AFLF may allow for identification of ultrastructural features of paramyxovirus as the etiologic agent, aid in clinical management, and assist in determination of prognosis.

1962 Ultrastructural Features of Gelophyisic Dysplasia: Role of Electron Microscopy in Diagnosis

J Hicks, JP Barrish, SH Zhu, N Brunetti-Pierri. Texas Children's Hospital & Baylor College of Medicine, Houston, TX; Baylor College of Medicine, Houston, TX.

Background: Geleophysic Dysplasia (GD), an autosomal recessive disorder, is a member of the Acromelic Dysplasia Group, which includes Weill-Marchesani Syndrome and Acromicric Dysplasia. All 3 disorders are characterized by short stature, short hands, stiff joints, delayed bone age, cone-shaped epiphyses, thick skin and heart disease. Molecular testing is in the development phase and of considerable expense. GD is a lysosomal storage disease that may be identified by electron microscopy of cultured fibroblasts.

Design: 8 children with clinically suspected GD underwent skin punch biopsies to establish fibroblast cultures for electron microscopic examination, and for future genetic and molecular testing. The study population consisted of 5 males and 3 females with an age range from 13 months to 13 years. Fibroblasts were harvested from the cell cultures, and prepared for electron microscopic examination. 4 skin cell cultures of normal fibroblasts were examined as controls.

Results: Light microscopic examination of the semi-thin sections of the cultured normal and GD fibroblasts showed cellular specimens. The fibroblasts were round to ovoid in outline and had a moderate amount of cytoplasm. The nuclei tended to have indented

surfaces and were somewhat irregular in outline. There was adequate preservation for electron microscopic examination. Both normal and GD fibroblasts showed a mild to moderate degree of rough endoplasmic reticulum dilation with granular material present. The normal fibroblasts had typical cell organelles. GD fibroblasts possessed frequent lysosomal storage vacuoles. These lysosomes contained lamellar structures which vaguely resembled myelin-like figures, which are characteristic for GD. Such structures were absent in all normal fibroblasts.

Conclusions: ADAMTSL2 gene and 6 other genes within a critical interval on chromosome 9q34.2-q34.3 have been linked to Geleophysic Dysplasia. ADAMSTL2 is involved in microfibrillar networks, and mutations lead to reduced secretion of the proteins and misfolding of mutated ADAMTSL2 proteins. ADAMTSL2 interacts with latent TGF-beta-binding protein-1 nuclear localization of phosphorylated SMAD2, a regulator of cell growth and apoptosis. Electron microscopic detection of lysosomes containing lamellar structures in GD fibroblasts, most likely represents mutated ADAMTSL2 protein and an attempt to degrade the mutated protein. Electron microscopy plays a crucial role in GD diagnosis.

1963 Cellular Neurothekeoma: Ultrastructural Features and Comparison with Plexiform Fibrohistiocytic Tumor

J Hicks, E Wartchow, J Barrish, SH Zhu, L Goin, J Schrieber, G Mierau. Texas Children's Hospital & Baylor College of Medicine, Houston, TX; The Children's Hospital, Aurora, CO.

Background: Cellular neurothekeoma (CNK) is a benign cutaneous neoplasm that affects children and young adults and occurs in the upper extremity, and head and neck. Similarly, plexiform fibrohistiocytic tumor (PFHT) is a cutaneous tumor affecting children and young adults in a similar pattern. In contrast, PFHT tends to recur locally and has metastatic potential (low-grade malignancy). CNK and PFHT share certain histopathologic and immunocytochemical features, leading to difficulty in separating a benign (CNK) tumor from a low-grade malignancy (PFHT).

Design: Patient population consisted of 6 children with CNK (4F:2M, age range 2-10 yrs) and 6 children with PFHT (4F:2M, age range 4 mos-8 yrs). Sites of involvement were similar for CNK and PFHT (upper extremities, head, neck). Tissue was available for light microscopic and electron microscopic examination.

Results: CNK and PFHT shared similar histopathologic features with a plexiform architecture, and a mixture of spindled, epithelioid and "histiocytoid" cells. Occasional osteoclastic cells were noted with both CNK and PHFT. Mitotic activity was variable with both CNK and PFHT ranging from 1 to 22 per HPF. In cases where immunocytochemistry could be performed (CNK=5, PFHT=3), the immunophenotype was similar with positivity for vimentin, focal SMA, focal S100 and focal NSE. Electron microscopy demonstrated certain distinct, distinguishing differences between CNK and PFHT. CNKs were composed of epithelioid and spindled cells with occasional intercellular junctions. The spindle cell population had thin cell processes. CNK cells were surrounded by a thick moderately electron dense basal lamina material that separated the cells from each other. PFHTs were comprised of spindled to ovoid cells with a population of "histiocytoid" cells containing frequent lysosomal granules with "zebra body"-like inclusions, mimicking metabolic storage material. There was also a population of plump spindle cells with prominent endoplasmic reticulum, peripheral cytoplasmic filaments and discontinuous external lamina.

Conclusions: CNK and PFHT have very similar histopathologic and immunocytochemical features, although CNK is a benign tumor and PFHT is a malignant tumor that may metastasize to regional nodes or distant sites. Electron microscopic examination of these very similar tumors allows appropriate classification of these tumors and provides for appropriate management and follow-up.

1964 Experimental Segmental Glomerular Sclerosis with Capillary and Podocyte Cystic Dilatation – Electron Microscopic Studies

J Jackson, K Griffin, A Bidani, M Picken. Loyola Univ Med Ctr, Maywood.

Background: Focal and segmental glomerular sclerosis (FSGS) is the most frequent morphologic manifestation of glomerular injury seen in human biopsy material. Its etiology is diverse and the morphologic spectrum is not well defined. Recently, attemepts have been made to dissect FSGS into specific clinico-pathologic entities based on morphology. We previously reported on a distinct form of FSGS associated with experimental nephron reduction, podocyte toxicity and hypertension. Here, we report further electron microscopic (EM) studies of this model, which shed light on the capillary wall and podocyte contributions to the development of FSGS.

Design: Male rats (~250g, Harlan) underwent ½ and ¾ surgical nephrectomy, followed by a single dose of puromycin aminonucleoside (PAN)(75 mg/kg IP) 14 days after surgery. The animals were sacrificed at 4 weeks post PAN, and kidney pathology was evaluated using paraffin sections (H&E and PAS stains) as well as EM, using semithin and ultrathin sections.

Results: Animals developed massive proteinuria, hypertension and FSGS. While less than 10% of glomeruli showed classic FSGS, many more glomeruli (20-30% depending on the type of procedure) showed cystic changes within the tufts that were readily discernible in paraffin sections. These cystic spaces clustered within a single or adjacent glomerular segment(s). There was a spectrum of lesions ranging from segmental cystic dilatation to frank sclerosis. The earliest changes showed pure segmental cystic dilatation not associated with mesangial matrix increase or loss. Frequently, these cysts were seen first in the hilar region, either centrally or laterally. In more advanced lesions, an increase in mesangial matrix and capsular adhesions became apparent. While many cysts eventually became obliterated, some persisted into more advanced stages of sclerosis. Semithin Epon sections and further EM studies clearly demonstrated that while some of these cysts represented dilated glomerular capillaries, numerous pseudo-cysts developed within pododcytes. Their development was followed by the formation of capsular adhesions, which in turn formed a nidus for sclerosis.

Conclusions: In this model we have shown that the development of FSGS is preceeded by the development of abnormally-shaped capillary channels with capillary dilatation and characteristic cystic changes within podocytes. EM studies, in particular semithin sections, were very helpful in discerning the earliest lesions. If similar changes occur in humans, their early detection may be important for prevention.

1965 Newly Recognized Hepatic Lysosomal Storage Disorder Affecting Young Children

GW Mierau, EP Wartchow, AD Segura, LS Finn. The Children's Hospital, Denver, Aurora, CO; Children's Hospital of Wisconsin, Milwaukee, WI; Seattle Children's Hospital, Seattle, WA.

Background: A number of therapeutic agents (amiodarone, chloroquine, 4,4'-diethylaminoethoxyhexestrol, fluoxetine, gentamicin, perhexiline, tilorone) have been shown sometimes to produce lysosomal inclusions closely mimicking those associated with primary metabolic storage diseases. All such drug-induced inclusions described to date have presented either as membranous phospholipid whorls or as vesicles containing an amorphous flocculent material. We describe a third form of presumably drug-induced inclusion observed within the Kupffer cells of children.

Design: Electron microscopic examination of liver biopsy specimens from four children with complex incompletely defined medical conditons, ranging in age from 2 to12 years, was performed in an attempt to determine a cause for their hepatomegaly. All were experiencing chronic nutritional, immunologic, and infectious problems that had required a variety of drugs for control, and none exhibited clinical features suggestive of a primary metabolic storage disease.

Results: Observed within the Kupffer cells were multiple large irregularly shaped membrane bound inclusions packed with relatively small caliber (~25-35 nm) slightly curvilinear tubular structures. These inclusions do not correspond precisely in appearance to those of any known primary metabolic storage disease but are vaguely reminiscent of those associated with the late-infantile variant of neuronal ceroid lipofuscinosis.

Conclusions: The described inclusions are likely the product of a secondary storage phenomenon induced by an as yet unidentified therapeutic agent. Awareness of the existence of this type of inclusion may in some cases enable a costly diagnostic workup for a nonexistent genetic disease to be averted.

1966 Autophagy: A Unique Ultrastructural Feature of Hepatitis C Viral Hepatitis

SD Norwood, G Sidhu, N Cassai, G-Y Yang. Northwestern University Feinberg School of Medicine, Chicago, IL; New York University School of Medicine & New York VA Hospital, New York, NY.

Background: Typical histopathological features of chronic hepatitis C virus (HCV) infection are subtle bile duct damage, lymphocyte predominant portal tract inflammation, and mild steatosis. However, the effects of HCV on hepatocytes are uncertain. In vitro experiments have shown that HCV induced the accumulation of autophagosomes in immortalized human hepatocytes, without enhancing protein degradation by autophagosomes, probably indicating a defense mechanism to HCV infection . Here, we report direct evidence of the presence of autophagosomes seen on electron microscopy in HCV biopsy specimens, which were also correlated with HCV viral load, and histologic grade of hepatitis.

Design: 83 liver biopsy specimens, including 71 HCV and 12 non-HCV (5 hepatitis B, 5 cholestatic disease, and 2 autoimmune hepatitis), were analyzed histologically and ultrastructurally. Hepatitis C viral load and genotype were also determined.

Results: On electron microscopy, small double-membraned organelles located in the pericanalicular cytoplasm of hepatocytes and corresponding to autophagosomes (Figure 1) were found in 70 of 71 HCV cases, but not in non-HCV cases. Histologically, the affected hepatocytes lacked lipofuscin. 1 of the 71 HCV biopsies had no autophagosomes, exhibited a non-detectable HCV viral load (< 5,000 copies/ml), and showed extensive lipofuscin deposits. 7 of the 71 HCV biopsies had scanty autophagosomes (defined as < 3 autophagosomes per hepatocyte), exhibited low or non-detectable HCV viral loads (< 100,000 copies/ml), and had mild portal tract inflammation and fibrosis. The remaining HCV biopsies showed numerous autophagosomes (> 10 autophagosomes per hepatocyte), exhibited high viral loads (> 100,000 copies/ml), and most showed severe portal inflammation.

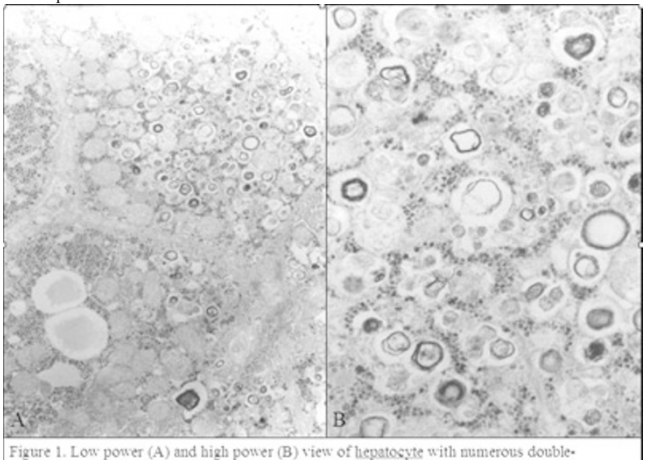

Figure 1. Low power (A) and high power (B) view of hepatocyte with numerous double-membrane bound autophagosomes.

Conclusions: Autophagosomes are a unique ultrastructural feature occurring in HCV-infected hepatocytes, and appear to be useful correlates of HCV viral load, intensity of inflammation and hepatocyte injury. The biological significance of autophagosomes in HCV needs to be further investigated, particularly for its role in HCV pathogenesis.

1967 NUT Midline Carcinoma: Diagnostic Ultrastructural Features

EP Wartchow, TS Moore, CA French, GW Mierau. The Children's Hospital, Aurora, CO; Brigham and Women's Hospital, Boston, MA.

Background: Nuclear protein in testis (NUT) midline carcinoma is a recently described entity which typically arises in children and young adults. NUT midline carcinomas tend to metastasize early, are almost uniformly lethal, and are most often characterized by a balanced t(15;19)(q13,p13.1) chromosomal translocation that results in a BRD4-NUT fusion oncogene. Although NUT midline carcinomas can be detected by cytogenetic and immunohistochemical means, electron microscopy remains a viable diagnostic tool. The electron microscopic (EM) findings associated with this highly aggressive tumor have thus far received only brief mention in the literature and have never previously been illustrated.

Design: The ultrastructural findings in a typical case of NUT midline carcinoma, confirmed by cytogenetic and fluorescence in situ hybridization studies, are presented to illustrate and characterize features which allow discrimination of this tumor from other entities with which this tumor is likely to be confused. Tissue from a thoracic mass arising in a 5-year-old child was fixed in glutaraldehyde and examined by electron microscopy. Representative micrographs were obtained and analyzed.

Results: Key ultrastructural findings included an often irregularly shaped nucleus containing one or more large nucleoli exhibiting a very prominent nucleonema, and an abundant electron dense cytoplasm containing numerous relatively short bundles of tonofilaments, clusters of pleomorphic granules, and deposits of lipid and glycogen. Stubby microvillous projections extended from the cell surfaces, and frequent punctate well formed desmosomal-type intercellular junctions were found. This constellation of features enables differentiation from thymic carcinoma, thymoma, germ cell tumor, Ewing's sarcoma, or mesothelioma.

Conclusions: Although NUT midline carcinomas are very aggressive tumors with a propensity for early hematogenous spread, they may be sensitive to specific chemotherapeutic regimens. NUT midline carcinoma displays a constellation of distinctive ultrastructural features which may allow earlier diagnosis and intervention. Electron microscopy can, particularly when genetic testing is unproductive or unavailable, prove helpful in discriminating NUT midline carcinoma from other similarly appearing entities.

1968 Hybrid Film/Digital Workflow in Electron Microscopy

CW Zuppan. Loma Linda University Medical Center, Loma Linda, CA.

Background: Newer electron microscopes utilize in-column digital cameras to initiate a total digital workflow for the imaging of electron microscopic findings. However, upgrading of existing older microscopes for digital image capture of sufficient quality for clinical diagnosis is expensive, on the order of $60,000 to $100,000. We have switched our laboratory from an all photographic to a hybrid film/digital workflow, and herein report our results.

Design: Our former full photographic workflow consisted of photographic development of large format film negatives, followed by traditional photographic enlargement and printing on 8 x 10 glossy photopaper. Our new hybrid workflow consists of photographic development of large format negatives, followed by scanning of negatives on a flatbed scanner, digital manipulation and labeling of the negatives in Photoshop, and printing of the final images on glossy 8 x 10 paper utilizing an ink-jet printer. As photographic development of the negatives was included in both our original (photographic) workflow and our new hybrid workflow, the time for that part of the process was not tracked.

Results: Post-negative time to final image was slightly longer with the hybrid workflow (6.3 versus 5.8 minutes/image), but personnel hands-on time was less (2.7 versus 5.8 minutes). Part of this time saving allowed for multitasking in the laboratory while some of the longer processes (scanning and final printing) were occurring. The quality of the final prints was subjectively improved, and the response of technical laboratory personnel to the new workflow was enthusiastic.

Conclusions: If upgrading to a full-digital image workflow is not financially feasible, we highly recommend transitioning to a hybrid film/digital workflow as an intermediary step. Overall time requirements are similar or slightly less than a full-photographic workflow, and consistent print quality is more easily achieved.